

Curvature Effects in Ocean Surface Scattering

Geir Engen, Ida Friestad-Pedersen, Harald Johnsen, and Tanos Elfouhaily

Abstract—Curvature effects in EM scattering from ocean surface are described using a generalized curvature expansion of the fields at an elevated nonperfect conducting surface. The new expansion formalism allows us to describe analytically and in general, without separating into different scales, the scattering of EM waves from an undulated ocean surface. The model is exact to first order in curvature for nonshadowing imaging geometry, and obeys the law of reciprocity and tilt invariance. Explicit expressions for EM fields at the surface, including both the projection and the self induced fields, are derived up to first order in surface curvature. Analytic closed form expressions for the scattered fields are derived from the surface field solutions, and applied to the case of backscattering, providing a general expression for the normalized radar cross section. The analytic expression for the normalized radar cross section is implemented for a linear surface model using both the Eulerian and the Lagrangian frame of reference. The results show that the model is capable of describing the expected dependency on polarization, incidence angle, and wind field with minimal restrictions in terms of range of validity. Comparison of polarization ratio shows good agreement between the model and measurements from the Envisat ASAR instrument.

Index Terms—Electromagnetic scattering, ocean surface, synthetic aperture radar.

I. INTRODUCTION

SATELLITES probing the Earth surface with electromagnetic waves (EM) will increase in both numbers and complexity within the coming years. Dedicated Earth observation (EO) satellites such as Radarsat-I and Envisat are already in operation, and new and even more advanced radar satellites are under preparation such as Radarsat-II, ALOS-PaISAR, and TerraSAR. In addition various constellations for utilizing sources of opportunity satellites such as the existing EO satellites, the GPS satellites, and the upcoming Galileo satellites will further increase the potential of EM probing of the Earth surface [1]–[4]. There is a wealth of information that possibly can be extracted from the EM scattered signal of ocean surfaces. Already demonstrated is the capabilities to extract geophysical information such as ocean gravity waves, surface winds, surface currents, and geoid [3], [5]–[7]. These are all parameters directly linked to the circulation of the ocean surface layer, and thus very important in climate modeling. Additionally these parameters are also of importance within marine meteorology and

operational oceanography. It is foreseen that new concepts of space-borne observation and new satellites will further improve the benefits of such observations in terms new products, higher quality, and better coverage. However, the interpretation of EM scattering from an ocean surface (stochastic dielectric) is not trivial in general, and requires treatment of both EM scattering and ocean surface wave statistics [8]. Of particular importance for future mission is the interpretation and utilization of dual-polarimetric measurements over ocean surfaces, such as provided by the Envisat ASAR Alt-Pol instrument. In that respect, the effect of the local surface curvature on the scattered signal plays a key role, and need to be modeled properly. With such knowledge, a combined analysis of both Doppler and radar cross section measurements in dual-polarization mode can be done with respect to retrieval of ocean surface features. This is believed to be the key issue for future utilization of space-borne Synthetic Aperture Radar (SAR) measurements in the modeling of ocean circulation in coastal areas.

Elementary wave scattering approximations were well developed and generalized before the end of the sixties. Two fundamental limits were hence identified: the low-frequency limit or the small perturbation method (SPM) [9] and the high-frequency limit or the Kirchhoff approximation (KA) [10]. These two limits were already generalized to be applicable to the full three-dimensional electromagnetic wave scattering from dielectric or penetrable surfaces. Shortly after, Lynch [11] had identified the need for curvature correction on the high-frequency limit or the Kirchhoff approximation (KA). His technique consisted of a variational method where the correct curvature terms can be found but in the restrictive context of scalar waves and quasispecular geometries. Rodriguez [12]–[14] have extended Lynch's technique to the vectorial electromagnetic waves but for perfectly conducting surfaces only. Rodriguez's model is termed the unified perturbation expansion (UPE). One of the major finding in the Rodriguez series of publications is the formal expression of curvature correction. The correction to KA is functionally a generalized curvature correction where all derivatives of the rough surface are involved through a Fourier kernel. Similar functional developments were also present in the tilt invariant approximation (TIA) [15] but for the acoustic Dirichlet boundary conditions. Both previous approaches are based on the extinction theorem which is as first principle as the Maxwell equations themselves. A more general approach was initiated by Voronovich [16]–[18] where similar curvature corrections were obtained even though the starting point is not the extinction theorem, per se, Voronovich [17] had reached a very general theory of diffraction by simply imposing some fundamental symmetry properties, such as reciprocity, shift invariance, and compliance with SPM to first and second orders. Voronovich's model is called the small-slope approximation (SSA) owing to the correspondence between orders of the model with orders of the slope and consequently curvature

Manuscript received July 11, 2003; revised December 2, 2005. This work was supported in part by the Research DG of the European Commission under contract EVG1-CT-2001-00051 and in part by the Norwegian Research Council under Contract 153781/420. The Envisat ASAR data were acquired under the Envisat AO project AOE-799.

G. Engen, I. Friestad-Pedersen, and H. Johnsen are with the Norut Information Technology Ltd., N-9294 Tromsø, Norway (e-mail: harald.johnsen@itek.norut.no).

T. Elfouhaily is with the Division of Applied Marine Physics, University of Miami Rosenstiel School of Marine and Atmospheric Science, Miami, FL 33149-1098 USA.

Digital Object Identifier 10.1109/TAP.2006.874309

for higher surface slopes. Another major difference between SSA and TIA or UPE is that the first SSA order is not the high-frequency limit of KA. SSA-1 is similar to KA but with the SPM-1 coefficients instead. This *a priori* minor difference has deep repercussions on the curvature kernel. Indeed, the kernel now might still have slope corrections which may enter in conflict with the curvature terminology. This subtlety was fully understood in the developments undertaken by Elfouhaily *et al.* [19]–[21]. It was demonstrated among other things, that if the tilt invariance is formally required then the curvature kernel can be induced. This model was termed the local curvature approximation (LCA). The procedure followed by Elfouhaily *et al.* [21] is similar to that by Voronovich [18] in a sense that symmetry properties were invoked instead of first principle equations such as Maxwell, Helmholtz, Stratton-Chu, etc.

In this paper, we intend to derive similar models such as UPE, TIA, SSA, LCA but by using the Stratton-Chu formalism [22], [23] to derive the surface current and the corresponding closed form expression for the scattered field. A generalized curvature expansion of the fields at a rough dielectric surface is performed. We will thus for simplicity call our method for GCM (generalized curvature method). The scattered EM-field is described up to first order solution in this generalized curvature kernel. This new development captures the effect of curvature on the scattering of EM waves from an ocean surface where both the projection fields and the self induced fields are included. The latter is important in order to properly describe the polarization effect of EM scattering from conducting curved surfaces.

Our derivation preserves the well known small perturbation method (SPM) and Kirchhoff approximation (KA) in its low and high frequency limits, respectively, and the model obeys the fundamental laws of reciprocity and tilt invariance. Multiple scattering and shadowing are not accounted for in this current development and hence both second order SPM and geometrical optics limits are not ensured. These previous limitations are not too stringent for ocean surface applications where most of the scattering happens locally, since the typical realistic sea surface slopes are always less than the highest radar incidence angle (50 degrees) considered in this study. This is also within the imaging geometry of typical space- or airborne SAR systems. The validity of the curvature model is solely connected to the radius of the curvature and the scattering angles, whenever nonlocal effects are negligible. For surfaces with Gaussian like spectra, which is the case for ocean surface, the key parameter is the correlation length [24]. The correlation length of the surface must be much longer than the radar wavelength. Since the radar wavelength of interest here is around 5 cm (C-band), and the sea surface correlation length is typical around 2.4 m (for wind speed of 6 m/s) [25], the validity of the curvature expansion is obtained.

The theoretical derivations are described in Section II where we start by describing in Section II-B the general curvature expansion. In Section II-B.1 and Section II-B.2 we solve explicitly for the EM field on the surface up to first order in curvature.

The solutions for the fields on the surface are then in Section III used to derive a closed form expression for the scattered EM field.

In Section IV we have applied the results of Section III to the special case of backscattering at C-band from an ocean surface,

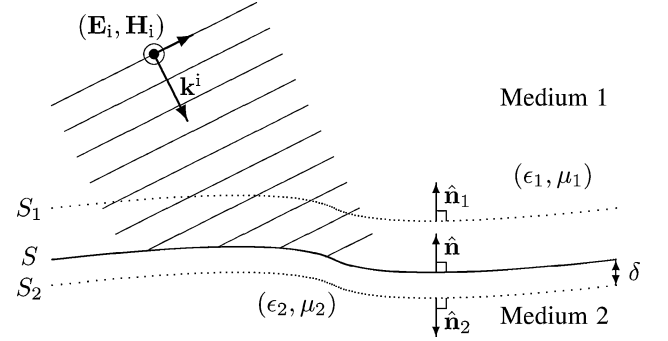


Fig. 1. Boundary surface between Medium 1 (air) and Medium 2 (ocean).

and derived expression for the ensemble-averaged normalized radar backscatter cross-section. Based on this, a numerical implementation is done.

In Section V numerical results are shown for different polarizations, wind speeds and incidence angles. Comparison with existing semi-empirical model (CMOD) [26], [27] is done for the VV polarization. The predicted polarization ratio is compared with existing models [28], [29] and measurements from the Envisat ASAR AP instrument.

II. SURFACE FIELD

A. Background Theory

The general problem of finding the EM-field at a boundary surface is illustrated by Fig. 1, where we have an EM plane-wave ($\mathbf{k}^i, \tilde{\mathbf{E}}_i, \tilde{\mathbf{H}}_i$) incident on an interface S between two media with different dielectric constant, ϵ , and/or different magnetic permeabilities μ . We assume ϵ and μ to be constant for any position \mathbf{r} inside the same medium. On both sides of the interface the dynamic conditions given by Maxwell's equations must be satisfied for the total field ($\tilde{\mathbf{E}}, \tilde{\mathbf{H}}$), and at the interface S the boundary condition requiring that $\hat{\mathbf{n}} \cdot \epsilon \tilde{\mathbf{E}}, \hat{\mathbf{n}} \cdot \mu \tilde{\mathbf{H}}, \hat{\mathbf{n}} \times \tilde{\mathbf{E}}$ and $\hat{\mathbf{n}} \times \tilde{\mathbf{H}}$ are continuous. Here $\hat{\mathbf{n}}$ is the unit normal vector of S .

Equivalent to satisfying Maxwell's differential equations, is to satisfy the Stratton-Chu [22], [23] integral equations for an observation point \mathbf{r} on an integration surface S_1 or S_2 for Medium 1 or 2, respectively. We will thus establish the Stratton-Chu equations for the EM fields at the surfaces S_1 and S_2 , and letting S_2 approach the boundary surface S . We can then solve for the EM fields at the surface S using the boundary conditions and by performing a generalized curvature expansion of the fields. Without loss of generality, we can define the complex envelope (\mathbf{E}, \mathbf{H}) of the total EM-field trough

$$(\mathbf{E}, \mathbf{H})(\mathbf{r}) \equiv (\tilde{\mathbf{E}}, \tilde{\mathbf{H}})(\mathbf{r}, t) e^{i\mathbf{k}^i \cdot \mathbf{r} - i\omega t} \quad (1)$$

where ω is the angular frequency and \mathbf{k}^i is the wave vector of the incident wave, and write the Stratton-Chu for the magnetic field of Medium 1 on the following form:

$$\begin{aligned} \mathbf{H}(\mathbf{r}) = & 2\mathbf{H}_i + 2 \int_S dS' e^{i\mathbf{k}^i \cdot (\mathbf{r} - \mathbf{r}')} \\ & \times \left\{ i\omega\epsilon_1 G_1(\mathbf{r} - \mathbf{r}') \hat{\mathbf{n}}(\mathbf{r}') \times \mathbf{E}(\mathbf{r}') \right. \\ & + (\hat{\mathbf{n}}(\mathbf{r}') \times \mathbf{H}(\mathbf{r}')) \times \nabla' G_1(\mathbf{r} - \mathbf{r}') \\ & \left. + \hat{\mathbf{n}}(\mathbf{r}') \cdot \mathbf{H}(\mathbf{r}') \nabla' G_1(\mathbf{r} - \mathbf{r}') \right\} \quad (2) \end{aligned}$$

where the Green's function is given by

$$G_\alpha(\mathbf{r} - \mathbf{r}') = \frac{e^{-i\alpha k_r |\mathbf{r} - \mathbf{r}'|}}{4\pi |\mathbf{r} - \mathbf{r}'|} \quad (3)$$

with $\alpha = 1$ and the radar wave-number of medium 1 as $k_r = |\mathbf{k}^i| = \omega\sqrt{\epsilon_1\mu_1}$.

We then let S_2 approach S ($\delta \rightarrow 0$). The Stratton-Chu equation for Medium 2 will then in combination with the boundary conditions, give the following new relation for the Medium 1 field (\mathbf{E}, \mathbf{H}) at the surface S

$$\begin{aligned} \mathbf{H}(\mathbf{r}) = & -2 \int_S dS' e^{i\mathbf{k}^i \cdot (\mathbf{r} - \mathbf{r}')} \\ & \times \left\{ i\omega\epsilon_2 G_\nu(\mathbf{r} - \mathbf{r}') \hat{\mathbf{n}}(\mathbf{r}') \times \mathbf{E}(\mathbf{r}') \right. \\ & + (\hat{\mathbf{n}}(\mathbf{r}') \times \mathbf{H}(\mathbf{r}')) \times \nabla' G_\nu(\mathbf{r} - \mathbf{r}') \\ & \left. + \frac{\mu_1}{\mu_2} \hat{\mathbf{n}}(\mathbf{r}') \cdot \mathbf{H}(\mathbf{r}') \nabla' G_\nu(\mathbf{r} - \mathbf{r}') \right\} \quad (4) \end{aligned}$$

where $\nu \equiv \sqrt{\epsilon_2\mu_2/\epsilon_1\mu_1}$ is the complex reflection index between the two media. The latter equation will in the following be used to iteratively give boundary conditions for the EM-field at the interface S . In the following we will assume that $\mu_2 = \mu_1$, which holds for the air-water interface.

B. Curvature Expansion

The basic idea of the (generalized) curvature expansion is to solve the equation-set (2), (4) with respect to the electromagnetic field on S_1 by expanding the field into different order of (generalized) curvature of the surface S and then solve each order separately. For the fields inside the integrals of the equation-set, the shift in position: $\mathbf{r}' - \mathbf{r}$, generates additional curvature terms since the surface slope \mathbf{s}' in position \mathbf{r}' may be different from the slope $\mathbf{s} \equiv \nabla\eta$ in position \mathbf{r} . We thus have for the fields

$$\{\mathbf{H}(\mathbf{r}')\}^{(0)} = \mathbf{H}^{(0)}(\mathbf{s}) \quad (5)$$

$$\{\mathbf{H}(\mathbf{r}')\}^{(1)} = \mathbf{H}^{(1)}(\mathbf{r}'; \mathbf{s}) + (\mathbf{s}' - \mathbf{s}) \cdot \frac{\partial}{\partial \mathbf{s}} \mathbf{H}^{(0)}(\mathbf{s}) \quad (6)$$

$$\begin{aligned} \{\mathbf{H}(\mathbf{r}')\}^{(2)} = & \mathbf{H}^{(2)}(\mathbf{r}'; \mathbf{s}) + (\mathbf{s}' - \mathbf{s}) \cdot \frac{\partial}{\partial \mathbf{s}} \mathbf{H}^{(1)}(\mathbf{r}'; \mathbf{s}) \\ & + \frac{1}{2} (\mathbf{s}' - \mathbf{s})(\mathbf{s}' - \mathbf{s}) : \frac{\partial^2}{\partial \mathbf{s} \partial \mathbf{s}} \mathbf{H}^{(0)}(\mathbf{s}). \quad (7) \end{aligned}$$

The same expansion is also used for the vector-fields: \mathbf{E} and $\hat{\mathbf{n}}$. The upper indexes indicates the order of (generalized) curvature. The position differences are expanded in the following way:

$$\{\mathbf{r}' - \mathbf{r}\}^{(0)} = (\mathbf{I} + \hat{\mathbf{z}}\nabla\eta(\mathbf{x})) \cdot \mathbf{x}'' \equiv \mathbf{r}'' \quad (8)$$

$$\begin{aligned} \{\mathbf{r}' - \mathbf{r}'\}^{(1)} = & \mathbf{r}' - \mathbf{r} - \mathbf{r}'' \\ = & \hat{\mathbf{z}}(\eta(\mathbf{x}') - \eta(\mathbf{x}) - \nabla\eta(\mathbf{x}) \cdot \mathbf{x}'') \quad (9) \end{aligned}$$

$$\{\mathbf{r}' - \mathbf{r}'\}^{(2)} = 0. \quad (10)$$

Here $\mathbf{x}'' = \mathbf{x}' - \mathbf{x}$ is the horizontal components of \mathbf{r}'' , where \mathbf{x}' and \mathbf{x} are the horizontal components of \mathbf{r}' and \mathbf{r} , respectively, and \mathbf{I} is the identity tensor. We shall in the next sub-sections use the above expansion to derive the zero and first order curvature solutions of (2) and (4).

1) *Zero Order Curvature Solution:* If we approximate S by its tangential plane $S_{||}$ in \mathbf{r} , or equivalently if the surface itself contains no curvature, the fields inside the integrals of (2) and (4) can be written as

$$\mathbf{E}(\mathbf{r}') = \mathbf{E}(\mathbf{r}), \quad \mathbf{H}(\mathbf{r}') = \mathbf{H}(\mathbf{r}), \quad \hat{\mathbf{n}}(\mathbf{r}') = \hat{\mathbf{n}}(\mathbf{r}). \quad (11)$$

The solution ($\mathbf{E}^{(0)}, \mathbf{H}^{(0)}$) of applying the assumption above, represents the tangent-plane solution. With those assumptions, all fields and normal vectors can be put outside the integrals and (2) takes the form

$$\begin{aligned} \mathbf{H}^{(0)} = & 2\mathbf{H}_i + 2i\omega\epsilon_2 \hat{\mathbf{n}} \times \mathbf{E}^{(0)} \int_{S_{||}} d\mathbf{x}'' e^{-i\mathbf{k}^i \cdot \mathbf{x}''} G_1(\mathbf{r}'') \\ & + 2(\hat{\mathbf{n}} \times \mathbf{H}^{(0)}) \times \int_{S_{||}} d\mathbf{x}'' e^{-i\mathbf{k}^i \cdot \mathbf{x}''} \nabla'' G_1(\mathbf{r}'') \\ & + 2\hat{\mathbf{n}} \cdot \mathbf{H}^{(0)} \int_{S_{||}} d\mathbf{x}'' e^{-i\mathbf{k}^i \cdot \mathbf{x}''} \nabla'' G_1(\mathbf{r}'') \quad (12) \end{aligned}$$

where \mathbf{r}'' is the new integration variable. A similar zero-order curvature relation can be found from (4). By using the integral identity [30]

$$\int_{\mathbb{R}^2} dae^{-i\mathbf{b} \cdot \mathbf{a}} \frac{e^{-i b_0 \sqrt{a_0^2 + |\mathbf{a}|^2}}}{4\pi \sqrt{a_0^2 + |\mathbf{a}|^2}} = \frac{e^{i|a_0| \sqrt{b_0^2 - |\mathbf{b}|^2}}}{2i \sqrt{b_0^2 - |\mathbf{b}|^2}} \quad (13)$$

we get the following set of linear equations to solve for the EM fields:

$$\left\{ \mathbf{I} - \frac{\mathbf{q}^i \hat{\mathbf{n}} - \hat{\mathbf{n}} \mathbf{q}^i}{p_1^i} \right\} \cdot \mathbf{H}^{(0)} = 2\mathbf{H}_i + \frac{\omega\epsilon_1}{k_r p_1^i} \hat{\mathbf{n}} \times \mathbf{E}^{(0)} \quad (14)$$

$$\left\{ \mathbf{I} + \frac{\mathbf{q}^i \hat{\mathbf{n}} - \hat{\mathbf{n}} \mathbf{q}^i}{\nu p_\nu^i} \right\} \cdot \mathbf{H}^{(0)} = -\frac{\omega\epsilon_2}{k_r \nu p_\nu^i} \hat{\mathbf{n}} \times \mathbf{E}^{(0)} \quad (15)$$

where the abbreviations: $\mathbf{q}^i \equiv \mathbf{q}(\mathbf{0})$, $p_1^i \equiv p_1(\mathbf{0})$ and $p_\nu^i \equiv p_\nu(\mathbf{0})$ are used for zero argument of the following functions:

$$\mathbf{q}(\mathbf{k}) \equiv \frac{\{\mathbf{I} - \hat{\mathbf{n}}\hat{\mathbf{n}}\} \cdot (\mathbf{k}^i - \mathbf{k})}{k_r} \quad (16)$$

$$p_\alpha(\mathbf{k}) \equiv \sqrt{1 - \frac{|\mathbf{q}(\mathbf{k})|^2}{\alpha^2}}. \quad (17)$$

Here, p_1^i and $q^i \equiv |\mathbf{q}^i|$, represents the cosines and sine of the local incidence angle, respectively, and $\hat{\mathbf{q}}^i \equiv \mathbf{q}^i/q^i$ represents the unit projection direction of the incidence radar wave vector onto the surface S (see Fig. 2). By solving the equation-set (14), (15) with respect to the orthogonal directions $\hat{\mathbf{q}}^i$, $\hat{\mathbf{w}}^i \equiv \hat{\mathbf{n}} \times \hat{\mathbf{q}}^i$ and $\hat{\mathbf{n}}$ of $\mathbf{H}^{(0)}$, we get:

$$\mathbf{H}^{(0)} = \left\{ \frac{2\hat{\mathbf{q}}^i \hat{\mathbf{q}}^i}{1 + \frac{p_1^i}{\nu p_\nu^i}} + \frac{2\hat{\mathbf{w}}^i \hat{\mathbf{w}}^i}{1 + \frac{p_\nu^i}{\nu p_1^i}} + \frac{2\hat{\mathbf{n}}\hat{\mathbf{n}}}{1 + \frac{\nu p_1^i}{p_1^i}} \right\} \cdot \mathbf{H}_i. \quad (18)$$

Rewriting (15), gives

$$\hat{\mathbf{n}} \times \mathbf{E}^{(0)} = -p_\nu^i \sqrt{\frac{\mu_2}{\epsilon_2}} \left\{ \mathbf{I} - \hat{\mathbf{n}}\hat{\mathbf{n}} + \frac{\mathbf{q}^i \mathbf{q}^i}{\nu^2 p_\nu^i{}^2} \right\} \cdot \mathbf{H}^{(0)}. \quad (19)$$

For the special cases when $|\nu|^2 \gg 1$ (e.g., Medium 1 is air and Medium 2 is water) we have that $p_\nu^i \rightarrow 1$ and (19) be-

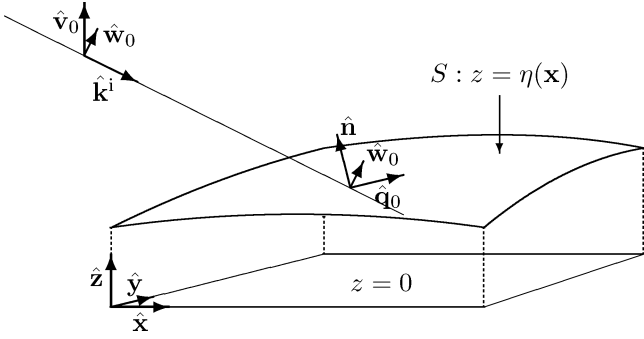


Fig. 2. Reference systems.

comes equal to the *Leontovich impedance boundary condition* [31]. The special case applies here since we operate at C-band (5.3 GHz) and the sea water conductivity is 4 S/m.

2) *First and Higher Order Curvature Solutions*: By using the curvature expansion of (7) and (9) for the vector fields and position offsets, respectively, and defining the n th-order transfer functions of the fields in the following way:

$$\mathbf{H}^{(n)}(\mathbf{x}; \mathbf{s}) = \int d\mathbf{k}_1 \dots \int d\mathbf{k}_n e^{i(\mathbf{k}_1 + \dots + \mathbf{k}_n) \cdot \mathbf{x}} \times T_{\mathbf{H}}^{(n)}(\mathbf{k}_1, \dots, \mathbf{k}_n; \mathbf{s}) \hat{\eta}(\mathbf{k}_1) \dots \hat{\eta}(\mathbf{k}_n) \quad (20)$$

the n th order generalized curvature versions of (2) and (4) can be written as

$$\left\{ \mathbf{I} - \frac{\mathbf{q}\hat{\mathbf{n}} - \hat{\mathbf{n}}\mathbf{q}}{p_1} \right\} \cdot T_{\mathbf{H}}^{(n)} = 2T_{\mathbf{H}_1^c}^{(n)} + \frac{\omega\epsilon_1}{k_r p_1} \hat{\mathbf{n}} \times T_{\mathbf{E}}^{(n)} \quad (21)$$

$$\left\{ \mathbf{I} + \frac{\mathbf{q}\hat{\mathbf{n}} - \hat{\mathbf{n}}\mathbf{q}}{\nu p_\nu} \right\} \cdot T_{\mathbf{H}}^{(n)} = -2T_{\mathbf{H}_\nu^c}^{(n)} - \frac{\omega\epsilon_2}{k_r \nu p_\nu} \hat{\mathbf{n}} \times T_{\mathbf{E}}^{(n)} \quad (22)$$

where the abbreviations: $\mathbf{q} = \mathbf{q}(\mathbf{k}_1 + \dots + \mathbf{k}_n)$ and $p_\nu = p_\nu(\mathbf{k}_1 + \dots + \mathbf{k}_n)$ are used for the functions defined in (16) and (17). $T_{\mathbf{H}_\alpha^c}^{(n)}$ is the n th order transfer function of the curvature source term

$$\begin{aligned} \mathbf{H}_\alpha^c(n) &\equiv \frac{i\omega\epsilon_1\alpha^2}{|\mathbf{n}|} \int_{S_{||}} d\mathbf{r}'' \left\{ e^{i\mathbf{k}^i \cdot (\mathbf{r} - \mathbf{r}')} \mathbf{n}' \times \mathbf{E}'^{(<n)} G_\alpha \right\}^{(n)} \\ &+ \frac{1}{|\mathbf{n}|} \int_{S_{||}} d\mathbf{r}'' \left\{ e^{i\mathbf{k}^i \cdot (\mathbf{r} - \mathbf{r}')} (\mathbf{n}' \times \mathbf{H}'^{(<n)}) \times \nabla' G_\alpha \right\}^{(n)} \\ &+ \frac{1}{|\mathbf{n}|} \int_{S_{||}} d\mathbf{r}'' \left\{ e^{i\mathbf{k}^i \cdot (\mathbf{r} - \mathbf{r}')} \mathbf{n}' \cdot \mathbf{H}'^{(<n)} \nabla' G_\alpha \right\}^{(n)}. \quad (23) \end{aligned}$$

Here the following short-hand notation is used for the Greens-function: $G_\alpha = G_\alpha(\mathbf{r} - \mathbf{r}')$ and the marks on the fields are used to indicate that the fields are given at position \mathbf{r}' . By the notation: $(\cdot)^{(<n)}$, we mean the sum of all order in curvature less than n . Explicit expressions for the transfer functions of \mathbf{H}_α^c are derived in Appendix A.

Solving equation-set (21), (22) with respect to $T_{\mathbf{H}}^{(n)}$ as a function of the curvature source term transfer functions, yields

$$\hat{\mathbf{q}} \cdot T_{\mathbf{H}}^{(n)} = \frac{2p_1}{q(1 + p_1/\nu p_\nu)} \hat{\mathbf{n}} \cdot \left\{ T_{\mathbf{H}_1^c}^{(n)} + T_{\mathbf{H}_\nu^c}^{(n)} \right\} \quad (24)$$

$$\hat{\mathbf{w}} \cdot T_{\mathbf{H}}^{(n)} = \frac{2}{1 + p_\nu/\nu p_1} \hat{\mathbf{w}} \cdot \left\{ T_{\mathbf{H}_1^c}^{(n)} - \frac{p_\nu}{\nu p_1} T_{\mathbf{H}_\nu^c}^{(n)} \right\} \quad (25)$$

$$\hat{\mathbf{n}} \cdot T_{\mathbf{H}}^{(n)} = \frac{2}{1 + \nu p_\nu/p_1} \hat{\mathbf{n}} \cdot \left\{ T_{\mathbf{H}_1^c}^{(n)} - \frac{\nu p_\nu}{p_1} T_{\mathbf{H}_\nu^c}^{(n)} \right\}. \quad (26)$$

From (22) we get the following impedance boundary condition for the n th order curvature term:

$$\begin{aligned} \hat{\mathbf{n}} \times T_{\mathbf{E}}^{(n)} &= -p_\nu \sqrt{\frac{\mu_2}{\epsilon_2}} \left\{ \mathbf{I} - \hat{\mathbf{n}}\hat{\mathbf{n}} + \frac{\mathbf{q}\mathbf{q}}{\nu^2 p_\nu^2} \right\} \cdot T_{\mathbf{H}}^{(n)} \\ &- p_\nu \sqrt{\frac{\mu_2}{\epsilon_2}} \left\{ \mathbf{I} - \hat{\mathbf{n}}\hat{\mathbf{n}} - \frac{\mathbf{q}\hat{\mathbf{n}}}{\nu p_\nu} \right\} \cdot 2T_{\mathbf{H}_\nu^c}^{(n)}. \quad (27) \end{aligned}$$

Since the leading term of $T_{\mathbf{H}_\nu^c}^{(1)}$ is $O(1/\nu)$ (see the results of next section), the criteria $|\nu|^2 \gg 1$ gives

$$\hat{\mathbf{n}} \times \mathbf{E}^{(1)} \approx \sqrt{\frac{\mu_2}{\epsilon_2}} \hat{\mathbf{n}} \times \hat{\mathbf{n}} \times \hat{\mathbf{H}}^{(1)}. \quad (28)$$

This shows that *Leontovich impedance boundary condition* holds for the case of air/sea interface up to first order in curvature. However, we will in the derivation of the scattered field, use the general expression given by (27).

III. SCATTERED FIELD

The curvature solutions of the fields on the surface S as given in Section II-B.1 and Section II-B.2 are now used to derive expression for the scattered magnetic field. The scattered magnetic field in position \mathbf{r}' (above the surface) can be expressed by the complex envelopes of the electric and magnetic surface currents using Frans formula [23], [32]

$$\begin{aligned} \tilde{\mathbf{H}}(\mathbf{r}') &= \nabla' \times \nabla' \times \frac{i}{\omega\mu} \int dS e^{-i\mathbf{k}^i \cdot \mathbf{r}} \mathbf{J}_m(\mathbf{r}) G_1(\mathbf{r} - \mathbf{r}') \\ &+ \nabla' \times \int dS e^{-i\mathbf{k}^i \cdot \mathbf{r}} \mathbf{J}_e(\mathbf{r}) G_1(\mathbf{r} - \mathbf{r}') \quad (29) \end{aligned}$$

where the complex envelope of the electric and magnetic surface currents are defined by: $\mathbf{J}_e \equiv \hat{\mathbf{n}} \times \mathbf{H}$ and $\mathbf{J}_m \equiv \hat{\mathbf{n}} \times \mathbf{E}$, respectively.

In the Fraunhofer zone (far field zone) the complex envelope of the relative scattered magnetic field, at a given polarization $\hat{\mathbf{H}}_s$, becomes

$$\frac{\hat{\mathbf{H}}_s \cdot \mathbf{H}(\mathbf{r}')}{|\mathbf{H}_i|} = \frac{ik_r}{4\pi r_0} \int_A d\mathbf{x} e^{-i\mathbf{k}^i \cdot \mathbf{x} - i\mathbf{k}^s \cdot \eta(\mathbf{x})} \mathcal{F}(\mathbf{x}) \quad (30)$$

where r_0 is the distance between the radar platform and the center of the illuminated area \mathcal{A} , $\mathbf{k}^- = \mathbf{k}^i - \mathbf{k}^s$ is the difference between the incidence and scattered wave-vectors \mathbf{k}^i and \mathbf{k}^s , and

$$\mathcal{F} \equiv -\frac{|\mathbf{n}|}{|\mathbf{H}_i|} \hat{\mathbf{H}}_s \cdot \left\{ \frac{k_r}{\omega\mu} \hat{\mathbf{k}}^s \times \hat{\mathbf{k}}^s \times \mathbf{J}_m + \hat{\mathbf{k}}^s \times \mathbf{J}_e \right\}. \quad (31)$$

Here $\hat{\mathbf{k}}^s$ is the unit scattering direction vector. Combining this with the results of the curvature expansion done in the previous chapter it is natural to write \mathcal{F} as

$$\mathcal{F}(\mathbf{x}) = F^{(0)}(\mathbf{s}) + F^{(1)}(\mathbf{x}; \mathbf{s}) + F^{(2)}(\mathbf{x}; \mathbf{s}) + \dots \quad (32)$$

where $F^{(n)}$ represents the n th order generalized curvature term coming from substituting the expressions for the complex envelopes of the total surface currents in (31) with $\mathbf{J}_m^{(n)} = \hat{\mathbf{n}} \times \mathbf{E}^{(n)}$

and $\mathbf{J}_e^{(n)} = \hat{\mathbf{n}} \times \mathbf{H}^{(n)}$. Before going any further in the development of the theory, we need to keep in mind what is causing the different order in generalized curvature of the surface EM-field: the zero order curvature term represents the projection of the incoming field onto the surface whereas the first and higher order terms represent the self induced EM-field on the surface.

A. Geometric Curvature Expansion

Since \mathcal{F} is inside the scattering integral of (30) the self induced field is not the only effect expandable in terms of generalized curvature. The same expansion can be done with the geometric effects caused by the slope dependence of the fields. Instead of writing \mathcal{F} on the form given in (32), where we have an explicit dependence of the slope, we want to find a new representation

$$\mathcal{F}(\mathbf{x}) = \mathcal{F}^{(0)} + \mathcal{F}^{(1)}(\mathbf{x}) + \mathcal{F}^{(2)}(\mathbf{x}) + \dots \quad (33)$$

with no explicit slope dependence, and where the n th order term represents the n th order in generalized curvature of the combination of self-induced and geometric effects.

1) *Zero Order Term:* Given the scattering integral of (30)

$$\mathcal{F}^{(0)} \equiv F^{(0)} \left(-\frac{\mathbf{k}h^-}{k_z^-} \right) \quad (34)$$

represents the zeroth order generalized curvature term. The remaining terms are clearly of order one or higher in generalized curvature, since a Taylor expansion of $F^{(0)}(\mathbf{s})$ around $\mathbf{s} = \mathbf{0}$ in combination with integration by part, gives the following relation:

$$F^{(0)}(\mathbf{s}) - F^{(0)} \left(-\frac{\mathbf{k}h^-}{k_z^-} \right) \sim \int d\mathbf{k} e^{i\mathbf{k} \cdot \mathbf{x}} T_{\Delta}^{(1)}(\mathbf{k}; \mathbf{s}) \hat{\eta}(\mathbf{k}) \quad (35)$$

where

$$T_{\Delta}^{(1)}(\mathbf{k}; \mathbf{s}) = i\mathbf{k}\mathbf{k} : \sum_{n=2}^{\infty} \frac{\nabla_{\mathbf{s}}^n F^{(0)}(\mathbf{0})}{n!} : \sum_{m=0}^{n-2} \frac{m+1}{k_z^-} \mathbf{s}^m \left(\frac{-\mathbf{k}h^-}{k_z^-} \right)^{n-2-m} \quad (36)$$

This relation is valid inside the scattering integral when $|\mathcal{A}| \rightarrow \infty$ (i.e neglecting the contribution from the border of the illuminated area). By setting $\mathbf{s} = -\mathbf{k}_h^-/k_z^-$ for the $F^{(0)}$ term of the scattering integral, the order is *terminated* to zero order in generalized curvature.

2) *First Order Term:* The transfer function of the first order term

$$\mathcal{F}^{(1)}(\mathbf{x}) = \int d\mathbf{k} e^{i\mathbf{k} \cdot \mathbf{x}} T_{\mathcal{F}}^{(1)} \hat{\eta}(\mathbf{k}) \quad (37)$$

is given by the sum of $T_{\mathcal{F}}^{(1)}$ and the remaining part from the zero order termination of $F^{(0)}$

$$T_{\mathcal{F}}^{(1)}(\mathbf{k}) = T_{\mathcal{F}}^{(1)} \left(\mathbf{k}; \frac{\mathbf{k} - \mathbf{k}_h^-}{k_z^-} \right) + T_{\Delta}^{(1)} \left(\mathbf{k}; \frac{\mathbf{k} - \mathbf{k}_h^-}{k_z^-} \right) \quad (38)$$

where the first order termination $\mathbf{s} = (\mathbf{k} - \mathbf{k}_h^-)/k_z^-$ is used. With this termination, $T_{\Delta}^{(1)}$ can be written as

$$T_{\Delta}^{(1)} \left(\mathbf{k}; \frac{\mathbf{k} - \mathbf{k}_h^-}{k_z^-} \right) = -ik_z^- F^{(0)} \left(\frac{\mathbf{k} - \mathbf{k}_h^-}{k_z^-} \right) + ik_z^- F^{(0)} \left(-\frac{\mathbf{k}_h^-}{k_z^-} \right) + i\mathbf{k} \cdot \nabla_{\mathbf{s}} F^{(0)} \left(\frac{\mathbf{k} - \mathbf{k}_h^-}{k_z^-} \right). \quad (39)$$

The remaining part of the first order termination can, in a similar way as for the zero order termination, be shown to yield terms of order two or higher in generalized curvature.

B. Explicit Expression for the Scattered Field

We will in this section give the expressions for the both the zero and first order generalized curvature terms for the general case of bi-static scattering. The results will be expressed by the radar reference frames, where the sets of orthogonal vectors $\{\hat{\mathbf{k}}^i, \hat{\mathbf{w}}^i, \hat{\mathbf{v}}^i\}$ and $\{\hat{\mathbf{k}}^s, \hat{\mathbf{w}}^s, \hat{\mathbf{v}}^s\}$ are representing the incidence and scattered geometry, respectively. The local vertical magnetic polarization vectors are given by $\hat{\mathbf{v}}^{i,s} \equiv \hat{\mathbf{k}}^{i,s} \times \hat{\mathbf{w}}^{i,s}$. The local angle Φ between the two reference frames are defined through $\cos \Phi = \hat{\mathbf{q}}^s \cdot \hat{\mathbf{q}}^i = \hat{\mathbf{w}}^s \cdot \hat{\mathbf{w}}^i$ and $\sin \Phi = \hat{\mathbf{q}}^s \cdot \hat{\mathbf{w}}^i = -\hat{\mathbf{w}}^s \cdot \hat{\mathbf{q}}^i$.

1) *Zero Order Term:* Setting in for $\hat{\mathbf{n}} \times \mathbf{H}^{(0)}$ and $\hat{\mathbf{n}} \times \mathbf{E}^{(0)}$ into (31), and using the zero order GCM termination condition, gives

$$\mathcal{F}^{(0)} = \hat{\mathbf{H}}_s \cdot \left\{ \mathcal{B}_{\text{vv}}^{(0)} \hat{\mathbf{v}}^s \hat{\mathbf{v}}^i + \mathcal{B}_{\text{ww}}^{(0)} \hat{\mathbf{w}}^s \hat{\mathbf{w}}^i \right\} \cdot \hat{\mathbf{H}}_i \quad (40)$$

where the coefficients are given by:

$$\mathcal{B}_{\text{vv}}^{(0)} = -\frac{2p_1^i}{n_z} \frac{1 - \frac{p_1^i}{\nu p_1^i}}{1 + \frac{p_1^i}{\nu p_1^i}} \quad (41)$$

$$\mathcal{B}_{\text{ww}}^{(0)} = \frac{2p_1^i}{n_z} \frac{1 - \frac{p_1^i}{\nu p_1^i}}{1 + \frac{p_1^i}{\nu p_1^i}} \quad (42)$$

Here, all the scalars p_1^i , p_1^s , and n_z , and the unit vectors $\hat{\mathbf{v}}^{i,s}$ and $\hat{\mathbf{w}}^{i,s}$ are to be computed with the termination condition: $\mathbf{s} = -\mathbf{k}_h^-/k_z^-$. The latter fractions in (41) and (42) are the well known reflection coefficients. Since $\mathbf{q}^i = \mathbf{q}^s$ and $p_{\alpha}^i = p_{\alpha}^s$ for this termination condition, the zero order term obviously satisfies the reciprocity property.

2) *First Order Term:* The first order generalized curvature transfer function $T_{\mathcal{F}}^{(1)}$ is given by (38) and (39), where the transfer function of $F^{(1)}$ is given by

$$T_{\mathcal{F}}^{(1)}(\mathbf{k}; \mathbf{s}) = -\frac{|\mathbf{n}|}{\mathbf{H}_i} \hat{\mathbf{H}}_s \cdot \left\{ \hat{\mathbf{k}}^s \times \hat{\mathbf{n}} \times T_{\mathbf{H}}^{(1)} + \frac{k_r}{\omega\mu} \hat{\mathbf{k}}^s \times \hat{\mathbf{k}}^s \times \hat{\mathbf{n}} \times T_{\mathbf{E}}^{(1)} \right\}. \quad (43)$$

Since $\mathbf{q} \rightarrow \mathbf{q}^s$ and $p_{\alpha} \rightarrow p_{\alpha}^s$ with the first order generalized curvature termination condition: $\mathbf{s} = (\mathbf{k} - \mathbf{k}_h^-)/k_z^-$, the transfer function of the first order generalized curvature term $\mathcal{F}^{(0)}$ can be written as

$$T_{\mathcal{F}}^{(1)}(\mathbf{k}) = ik_z^- \mathcal{F}^{(0)} + \hat{\mathbf{H}}_s \cdot \left\{ \mathcal{B}_{\text{vv}}^{(1)} \hat{\mathbf{v}}^s \hat{\mathbf{v}}^i + \mathcal{B}_{\text{ww}}^{(1)} \hat{\mathbf{w}}^s \hat{\mathbf{w}}^i + \mathcal{B}_{\text{vv}}^{(1)} \hat{\mathbf{v}}^s \hat{\mathbf{v}}^i + \mathcal{B}_{\text{ww}}^{(1)} \hat{\mathbf{w}}^s \hat{\mathbf{w}}^i \right\} \cdot \hat{\mathbf{H}}_i \quad (44)$$

where the coefficients are given by

$$\mathcal{B}_{\text{VV}}^{(1)} = -4ik_{\mathbf{r}} \frac{(\nu^2 - 1)p_1^s p_1^i \cos \Phi}{(p_1^s + \nu p_1^s)(p_1^i + \nu p_1^i)} \quad (45)$$

$$\mathcal{B}_{\text{wv}}^{(1)} = 4ik_{\mathbf{r}} \frac{(\nu^2 - 1)p_1^s p_1^i (p_\nu^s p_\nu^i \cos \Phi - q^s q^i)}{(p_\nu^s + \nu p_1^s)(p_1^i + \nu p_1^i)} \quad (46)$$

$$\mathcal{B}_{\text{wv}}^{(1)} = -4ik_{\mathbf{r}} \frac{(\nu^2 - 1)p_\nu^s p_1^s p_1^i \sin \Phi}{(p_\nu^s + \nu p_1^s)(p_1^i + \nu p_1^i)} \quad (47)$$

$$\mathcal{B}_{\text{vw}}^{(1)} = 4ik_{\mathbf{r}} \frac{(\nu^2 - 1)p_\nu^i p_1^s p_1^i \sin \Phi}{(p_\nu^i + \nu p_1^i)(p_1^s + \nu p_1^s)}. \quad (48)$$

The $\mathcal{B}^{(1)}$ -coefficients, here computed at local incidence angles, are similar to the SPM1 results of Valenzuela [9]. The local incidence angles are given through the first order termination condition for the slopes. Except for $\mathcal{F}^{(0)}$ all quantities are to be computed with this termination condition. The results above means that $\mathcal{F}^{(1)}$ also satisfies the reciprocity property.

IV. COMPUTATION

A. The Normalized Radar Scattering Cross-Section

Expressions for the normalized radar cross-section (NRSC) can now be derived in terms of the scattered field and surface statistics. By using the definition of the normalized radar cross-section

$$\sigma^0 = \lim_{r_0 \rightarrow \infty} \frac{4\pi r_0^2}{|\mathcal{A}|} \left\langle \left| \frac{\hat{\mathbf{H}}_{\mathbf{r}} \cdot \tilde{\mathbf{H}}(\mathbf{r}_0)}{|\mathbf{H}_{\mathbf{i}}|} \right|^2 \right\rangle \quad (49)$$

where $|\mathcal{A}|$ is the horizontal size of the illuminated area and the operator $\langle \cdot \rangle$ represents the ensemble average, and assume statistical stationarity, we obtain

$$\sigma^0 = \frac{k_{\mathbf{r}}^2}{4\pi} \int d\mathbf{x} e^{-ik_{\mathbf{h}}^- \cdot \mathbf{x}} \times \left\langle e^{-ik_{\mathbf{z}}^- (\eta(\frac{\mathbf{x}}{2}) - \eta(-\frac{\mathbf{x}}{2}))} \mathcal{F}(\frac{\mathbf{x}}{2}) \mathcal{F}^* \left(-\frac{\mathbf{x}}{2}\right) \right\rangle. \quad (50)$$

Further, if we assume that the surface elevation field obeys Gaussian statistics, the Fourier kernel becomes

$$\begin{aligned} & \left\langle e^{-ik_{\mathbf{z}}^- (\eta(\frac{\mathbf{x}}{2}) - \eta(-\frac{\mathbf{x}}{2}))} \mathcal{F}(\frac{\mathbf{x}}{2}) \mathcal{F}^* \left(-\frac{\mathbf{x}}{2}\right) \right\rangle \\ &= e^{(k_{\mathbf{z}}^-)^2 (\phi_{\eta\eta}(\mathbf{x}) - \phi_{\eta\eta}(\mathbf{0}))} \\ & \times \left\{ \varphi_{\mathcal{F}^{(1)}\mathcal{F}^{(1)}}(\mathbf{x}) + \left(\mathcal{F}^{(0)} + ik_{\mathbf{z}}^- (\phi_{\mathcal{F}^{(1)}\eta}(\mathbf{x}) - \phi_{\mathcal{F}^{(1)}\eta}(\mathbf{0})) \right) \right. \\ & \left. \times \left(\mathcal{F}^{(0)*} - ik_{\mathbf{z}}^- (\phi_{\eta\mathcal{F}^{(1)}}(\mathbf{x}) - \phi_{\eta\mathcal{F}^{(1)}}(\mathbf{0})) \right) \right\} \quad (51) \end{aligned}$$

where the covariance functions $\phi_{\eta\eta}$, $\phi_{\mathcal{F}^{(1)}\eta}$, $\phi_{\eta\mathcal{F}^{(1)}}$, and $\phi_{\mathcal{F}^{(1)}\mathcal{F}^{(1)}}$ are defined by the following convention:

$$\phi_{ab}(\mathbf{x}) \equiv \left\langle \left(a\left(\frac{\mathbf{x}}{2}\right) - \langle a \rangle \right) \left(b\left(-\frac{\mathbf{x}}{2}\right) - \langle b \rangle \right)^* \right\rangle. \quad (52)$$

B. Numerical Computations

Equations (50) and (51) are now implemented for the case of backscattering, $\mathbf{k}^s = -\mathbf{k}^i$, and for two linear surface models—the usual Eulerian model and a Lagrangian model (described in Appendix B). Here, the model spectrum of Elfouhaily *et al.* [33] is used as the input wave-number spectrum needed

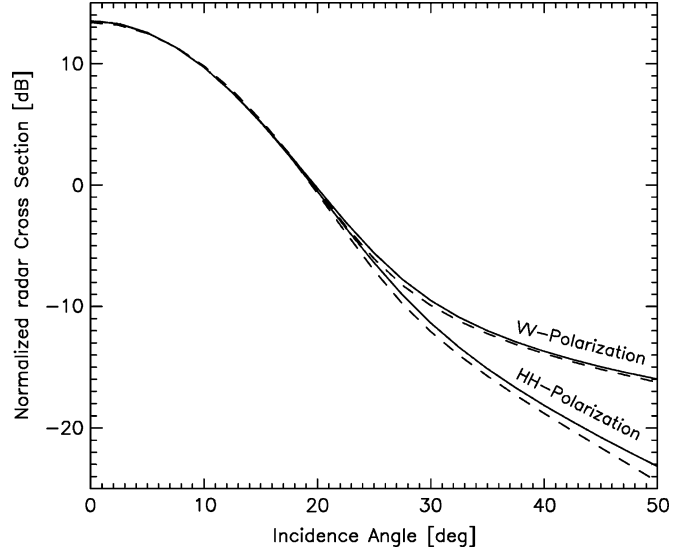


Fig. 3. Computed normalized radar cross section (NRCS) at C-band, VV and HH polarization for 10 m/s wind speed along the range (radar line of sight) direction. The lines are: Lagrangian surface model (solid) and Eulerian surface model (dashed).

in the computations of the covariances. This wave-spectrum is a closed form analytical model, derived for seas that are wind generated, and it is valid over all wave-numbers.

In the numerical computations, wavelengths ranging from 0.5 mm to 5 km are used. To efficiently compute the covariance functions for this wide range of wavelengths, the Fourier transforms are performed on a log-polar grid. The typical radar configurations used are: C-band (5.3 GHz), VV/HH polarization and incidence angles from 0° to 45° . The computations are performed for different wind speeds and wind directions. The sea water conductivity is set to 4 S/m.

V. RESULT

In this section we show the properties of the GCM, and perform a comparison of the NRCS and polarization ratio with semi-empirical model (CMOD-IF2) [26] and real data (Envisat ASAR). The CMOD-IF2 is a semi-empirical scattering model function derived for wind retrieval from ERS-1 Scatterometer instrument (C-band, 23 degree incidence angle) measurements of the ocean surface radar cross-section. The Envisat measurements are acquired in ASAR Alternating Polarization (AP) mode, and co-located with buoy or platform measurements. The ASAR data are acquired at three different locations (66.0 N, 8.1 E), (56.5 N, 3.2 E), (40.5 N, -69.43 E) and in the periods July–August 2003, and July–September 2004. Furthermore, the data are acquired in different swaths in order to have a larger range of incidence angles. The significant waveheight varies between 0.4 m–6.9 m with a mean value of 1.8 m. The wind speed varies between 2 m/s–18 m/s with a mean value of 6.2 m/s.

In Fig. 3, the NRCS as function of incidence angle is plotted for VV and HH polarizations using a Lagrangian and a Eulerian surface model. The use of Lagrangian surface model mimics weak nonlinearities in the wave field, and Fig. 3 quantifies the reduction in the dynamic range of the NRCS by introducing nonlinearities in the wave field.

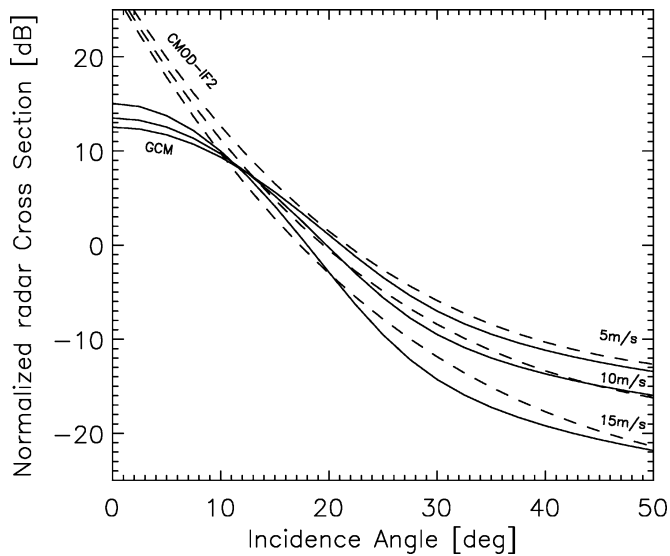


Fig. 4. Normalized radar cross section (NRCS) at C-band and VV polarization for wind speed of 5 m/s (upper), 10 m/s (middle) and 15 m/s (lower). The lines are: computed NRCS based on GCM using a Lagrangian surface model (solid) and CMOD-IF2 (dashed). The wind direction is along the range (radar line of sight) direction.

In Fig. 4 a comparison between the GCM and the semi-empirical CMOD-IF2 derived NRCS is shown for three different wind speeds for a range wind direction. Within the valid region of CMOD-IF2, we observe largest deviations in the range between 25 and 35 degree incidence angle where the GCM predicts lower values than the semi-empirical model. This discrepancy is most likely related to the surface model used. We see from Fig. 3 that introducing weak nonlinearities increase the predicted NRCS, but not sufficiently. This indicates that the probability of specular reflection is higher than predicted by the surface model used.

One of the main applications of the GCM function is to be able to better predict the polarization dependency in the NRCS from ocean surfaces. This is one of the major limitations of the existing semi-empirical models such as the CMOD [27]. The standard approach to predict the NRCS of HH polarization has been to use the CMOD in combination with a semi-empirical polarization ratio such as given by Thompson *et al.* [28].

In Fig. 5 the VV/HH polarization ratio of the predicted NRCS is plotted for different wind speeds and directions (relative to radar line-of-sight) as function of incidence angle, and overlaid measurements from Envisat ASAR AP data, as well as results of some existing models from literature. We see that the agreement is reasonably good, but for incidence angles between 27–33 degrees, our model predicts slightly higher values than the measurements. The GCM model predictions also agrees well with the semi-empirical model of Kudryavtsev *et al.* [34]. Fig. 5 also show that the GCM model performs better in predicting the VV/HH polarization ratio than the commonly used models from literature such as the model by Thompson *et al.* [28] and Elfouhaily [29]. Additionally the GCM model has built in both wind speed and wind direction dependency, which is not the case for the models of [28] and [29]. The deviation between GCM model and measurements for incidence angles between 27–33 degrees may come from imperfect calibration of

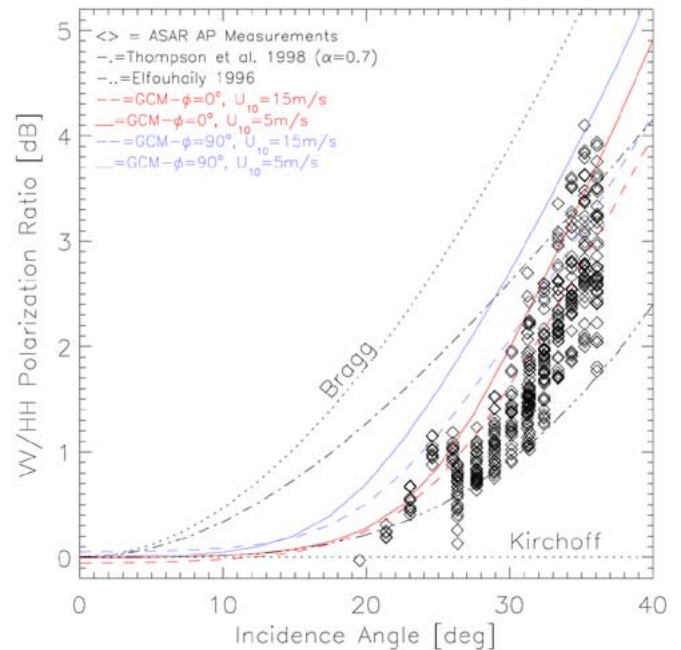


Fig. 5. VV/HH polarization ratio as function of incidence angle measured by Envisat ASAR AP instrument (C-band) and predicted by the GCM using a Lagrangian surface model. The red and blue lines represent computed ratio for range ($\phi = 0^\circ$) and azimuth ($\phi = 90^\circ$) wind direction, respectively, at two different wind speeds 5 m/s (dashed) and 15 m/s (solid). The polarization ratio of two existing models from literature [29] (dash-dot-dot) and [28] (dash-dot) are plotted for comparison together with the Bragg and Kirchoff limits (dotted).

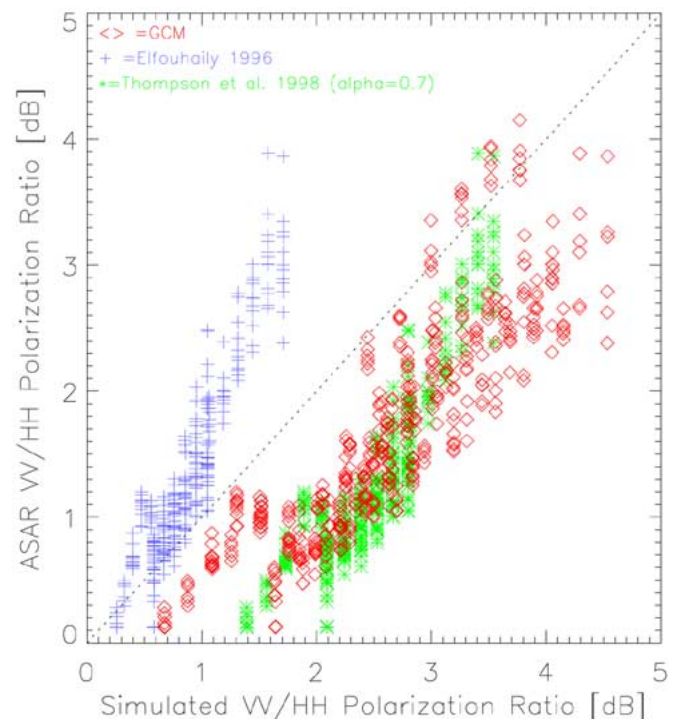


Fig. 6. VV/HH polarization ratio measured by Envisat ASAR AP instrument (C-band) versus computed ratios based on the GCM using a Lagrangian surface model. Simulations results based on two existing models from literature [28], [29] are plotted for comparison.

the ASAR AP data, since these points cover different sea-states (wind speed between 2–18 m/s). This is further likely to be the case since we can see some nongeophysical pattern in the data related to each swaths.

The in-situ data co-located with the ASAR AP measurements are used to simulate the VV/HH polarization ratio as predicted by various models. A comparison with measurements are shown in the scatter-plot of Fig. 6. The figure clearly shows that the GCM models better agrees with measurements than the existing models of literature. At low polarization ratios the agreement is good, while for higher ratios the deviations becomes significant. The deviations at higher polarization ratios (higher swaths) may come from a combination of reduced SNR of the ASAR instrument at higher incidence angles, imperfect calibration of the ASAR data, and limitations in the surface wave field description. The underestimation of specular reflection in the surface field description will bias the predicted VV/HH polarization ratio toward higher values.

VI. CONCLUSION

The motivation for this work was to develop a consistent formalism for describing EM scattering from an elevated nonperfect conducting curved surface. Expressions for the surface current and the corresponding scattered fields were derived using the Stratton-Chu formalism and a generalized curvature expansion of the fields at the surface. This new formalism allows us to analytically describe the scattering of EM waves from a curved surface, without separating into different scales. We derived explicit expressions for the surface EM fields, including both the projection and the self-induced fields, up to first order in surface curvature. Analytic closed form expressions for the scattered fields were then derived from the surface field solution by using the well known Frans Formula. For nonshadowing imaging geometries, the resulting model is exact to first order in surface curvature. Also, the model obeys the fundamental laws of reciprocity and tilt invariance, and it reproduces the SPM1 results of Valenzuela in the low frequency limit as well as the Kirchhoff approximation in the high frequency limit.

The formalism has been applied to the special case of backscattering, providing a general expression for the normalized radar cross section. A numerical implementation of the normalized radar cross section was done for two different surface models,—a linear Eulerian and a linear Lagrangian (Gerstner) surface model. Comparison of NRCS and polarization ratio show good agreement between the present model, semi-empirical CMOD-IF2 and measurements from Envisat ASAR AP data, respectively. Best agreement is obtained with the Lagrangian surface model, which mimics weak nonlinearities in the wave field. These results show that the model is capable of describing the expected dependency on polarization, wind speed and incidence angle with minimal restrictions in terms of range of validity. Furthermore, the model predicts the importance of wave statistics on the backscattering cross section. The observed deviation between the present model (GCM), CMOD-IF2 and ASAR AP data can be explained by the wave statistics, which has not been the topic for this paper, and possibly also by an imperfect calibration of the ASAR AP data. We believe that the remaining problem in terms of quantification of EM scattering from ocean surface is a proper statistical description of the ocean surface, especially the description and quantification of wave breaking effects [34]. This will be the topic and challenge for future studies.

APPENDIX

A. Derivation of the Source Functions

We will in this section give the first order source functions for dielectrics. By defining the following function:

$$\begin{aligned} A_\alpha^{(N,M)}(\mathbf{k}_1, \dots, \mathbf{k}_{N+M}; \mathbf{s}) &= \int_{S_{\parallel}} d\mathbf{r}'' e^{-i\mathbf{k}^i \cdot \mathbf{r}''} \left\{ \prod_{n=1}^N \left(e^{i\mathbf{k}_n \cdot \mathbf{r}''} - 1 \right) \right\} \\ &\times \left\{ \prod_{m=N+1}^{N+M} \left(e^{i\mathbf{k}_m \cdot \mathbf{r}''} - 1 - i\mathbf{k}_m \cdot \mathbf{r}'' \right) \right\} \\ &\times (\hat{\mathbf{z}} \cdot (\nabla'' - i\mathbf{k}^i))^M i k_r G_\alpha(\mathbf{r}'') \end{aligned} \quad (53)$$

and the following operator:

$$B_\alpha^{(N)} = \sum_{n=0}^N \frac{1}{n!(N-n)!} A_\alpha^{(n, N-n)} \prod_{m=1}^n i\mathbf{k}_m \cdot \frac{\partial}{\partial \mathbf{s}} \quad (54)$$

the first order source function can be written as

$$\begin{aligned} T_{\mathbf{H}_\alpha^c}^{(1)}(\mathbf{k}; \mathbf{s}) &= \sqrt{\frac{\epsilon_1}{\mu_1}} \alpha^2 n_z(\mathbf{s}) B_\alpha^{(1)}(\mathbf{k}; \mathbf{s}) \mathbf{n}(\mathbf{s}) \times \mathbf{E}^{(0)}(\mathbf{s}) \\ &- n_z(\mathbf{s}) \mathbf{B}_\alpha^{(1)}(\mathbf{k}; \mathbf{s}) \times \mathbf{n}(\mathbf{s}) \times \mathbf{H}^{(0)}(\mathbf{s}) \\ &+ n_z(\mathbf{s}) \mathbf{B}_\alpha^{(1)}(\mathbf{k}) \mathbf{n}(\mathbf{s}) \cdot \mathbf{H}^{(0)}(\mathbf{s}). \end{aligned} \quad (55)$$

The generalization to higher order in generalized curvature is straightforward. The \mathbf{B}_α operator is defined in the same way as B_α , where the corresponding \mathbf{A}_α is defined by performing the following substitution $i k_r G_\alpha \rightarrow \nabla'' G_\alpha$, in the last line of (53). The integral in this equation can be computed by using the integral identity of (13). By defining the following function:

$$L_\alpha^{(m)}(\mathbf{b}) = \left\{ \hat{\mathbf{z}} \cdot \left(i\mathbf{b} - i\mathbf{k}^i + \hat{\mathbf{n}} \frac{\partial}{\partial a_0} \right) \right\}^m i k_r \hat{G}_\alpha(\mathbf{b}, a_0) \Big|_{a_0=0} \quad (56)$$

where

$$\hat{G}_\alpha(\mathbf{b}, a_0) = \frac{e^{i|a_0| \sqrt{\alpha^2 k_r^2 - |\mathbf{b}|^2}}}{2i \sqrt{\alpha^2 k_r^2 - |\mathbf{b}|^2}} \quad (57)$$

we may write the A_α functions needed to compute the first order curvature source functions as

$$A_\alpha^{(1,0)}(\mathbf{k}; \mathbf{s}) = L_\alpha^{(0)}(k_r \mathbf{q}) - L_\alpha^{(0)}(k_r \mathbf{q}^i) \quad (58)$$

$$\begin{aligned} A_\alpha^{(0,1)}(\mathbf{k}; \mathbf{s}) &= L_\alpha^{(1)}(k_r \mathbf{q}) - L_\alpha^{(1)}(k_r \mathbf{q}^i) \\ &+ \mathbf{k}_{\parallel} \cdot \left(\nabla_{\mathbf{b}} L_\alpha^{(1)} \right) (k_r \mathbf{q}^i). \end{aligned} \quad (59)$$

In the exact similar way, can the \mathbf{A}_α functions be expressed by a set of \mathbf{L}_α functions defined by substituting $i k_r \rightarrow (i\mathbf{b} + \hat{\mathbf{n}}(\partial/\partial a_0))$ in the last line of (56).

B. Lagrangian Wave Description

A Lagrangian formulation describes the wave motion by following the individual fluid particles. This implies that the coordinate system moves and deforms with the fluid, unlike in the

Eulerian case where the coordinate system is fixed in space and time. Most analytical wave models are developed in the Eulerian frame of reference, but there are certain advantages to solving the equations of motion in the Lagrangian formulation and then transforming to Eulerian coordinates. Specifically, a linear Lagrangian solution will include some effects that are nonlinear in the Eulerian formulation. For instance, the Lagrangian solution will, when transformed to the Eulerian frame of reference, give a ‘‘Stokes-like’’ wave with steepened crests and flattened troughs. Also, some wave interactions (like how a short wave riding on a longer wave is modified by the longer wave, and as a result is longer and flatter in the troughs of the long wave than at the crests) are automatically included in the linear Lagrangian solution [35].

Let the surface elevation in Eulerian coordinates (\mathbf{x}) be $\eta(\mathbf{x})$, and assume that η at position \mathbf{x} can be written on the following form:

$$\eta(\mathbf{x}) = \tilde{\eta}(\tilde{\mathbf{x}})$$

where $\tilde{\mathbf{x}}$ is the solution of

$$\mathbf{x} = \tilde{\mathbf{x}} + \tilde{\boldsymbol{\xi}}(\tilde{\mathbf{x}}) \quad (60)$$

and the vector $\tilde{\boldsymbol{\chi}} = (\tilde{\boldsymbol{\xi}}, \tilde{\eta})$ represents the orbital motion of a fluid particle measured at the reference point $\tilde{\mathbf{x}}$. Solving the linearized equations of motion (Navier-Stokes) in Lagrangian coordinates will give the following result for $\tilde{\boldsymbol{\chi}}$ at the free surface

$$\tilde{\boldsymbol{\chi}}(\tilde{\mathbf{x}}) = \int d\mathbf{k} e^{i\mathbf{k} \cdot \tilde{\mathbf{x}}} T_{\tilde{\boldsymbol{\chi}}}(\mathbf{k}) \hat{\eta}(\mathbf{k}) \quad (61)$$

where

$$T_{\tilde{\boldsymbol{\chi}}}(\mathbf{k}) = (T_{\tilde{\boldsymbol{\xi}}}(\mathbf{k}), T_{\tilde{\eta}}(\mathbf{k})) = (i\hat{\mathbf{k}}, 1). \quad (62)$$

By changing to the Lagrangian reference system following the horizontal displacement $\tilde{\boldsymbol{\xi}}$ of the fluid-particles: $\mathbf{x} \rightarrow \tilde{\mathbf{x}} + \tilde{\boldsymbol{\xi}}$, the backscattered magnetic field can now be written as

$$\frac{\hat{\mathbf{H}}_s \cdot \mathbf{H}(\mathbf{r}')}{|\mathbf{H}_i|} = \frac{ik_r}{4\pi r_0} \int d\tilde{\mathbf{x}} e^{-i\mathbf{k}_h^- \cdot \tilde{\mathbf{x}} - i\mathbf{k}^- \cdot \tilde{\boldsymbol{\chi}}(\tilde{\mathbf{x}})} \tilde{\mathcal{F}}(\tilde{\mathbf{x}}) \tilde{\mathcal{F}}(\tilde{\mathbf{x}}) \quad (63)$$

where $\tilde{\mathcal{F}}$ is related to the surface current function \mathcal{F} in (30) by

$$\tilde{\mathcal{F}}(\tilde{\mathbf{x}}) = \mathcal{F}(\mathbf{x}) = \mathcal{F}(\tilde{\mathbf{x}} + \tilde{\boldsymbol{\xi}}) \quad (64)$$

and $\tilde{\mathcal{J}}$ is the Jacobian of the transformation, given by

$$\tilde{\mathcal{J}} = \det \begin{bmatrix} 1 + \frac{\partial \tilde{\xi}_x}{\partial \tilde{x}} & \frac{\partial \tilde{\xi}_y}{\partial \tilde{x}} \\ \frac{\partial \tilde{\xi}_x}{\partial \tilde{y}} & 1 + \frac{\partial \tilde{\xi}_y}{\partial \tilde{y}} \end{bmatrix}. \quad (65)$$

Like $\mathcal{F}(\mathbf{x})$, the function $\tilde{\mathcal{F}}(\tilde{\mathbf{x}})$ can be written as a sum

$$\tilde{\mathcal{F}}(\tilde{\mathbf{x}}) = \tilde{\mathcal{F}}^{(0)} + \tilde{\mathcal{F}}^{(1)}(\tilde{\mathbf{x}}) + \tilde{\mathcal{F}}^{(2)}(\tilde{\mathbf{x}}) + \dots \quad (66)$$

By using (64), it is possible to show that up to order 2

$$\tilde{\mathcal{F}}^{(0)} = \mathcal{F}^{(0)} \quad \text{and} \quad \tilde{\mathcal{F}}^{(1)}(\tilde{\mathbf{x}}) = \mathcal{F}^{(1)}(\tilde{\mathbf{x}}). \quad (67)$$

Also, the Jacobian $\tilde{\mathcal{J}}$ may be approximated by

$$\tilde{\mathcal{J}} \approx 1 + \nabla \cdot \tilde{\boldsymbol{\xi}}(\tilde{\mathbf{x}}) \equiv 1 + \tilde{\mathcal{J}}^{(1)}(\tilde{\mathbf{x}}). \quad (68)$$

From (63), it follows that the radar backscatter cross section in this case is:

$$\sigma^0 = \frac{k_r^2}{4\pi} \int d\tilde{\mathbf{x}} e^{-i\mathbf{k}_h^- \cdot \tilde{\mathbf{x}}} \left\langle e^{-i(\tilde{\zeta}(\frac{\tilde{\mathbf{x}}}{2}) - \tilde{\zeta}(-\frac{\tilde{\mathbf{x}}}{2}))} \times \tilde{\mathcal{J}}\left(\frac{\tilde{\mathbf{x}}}{2}\right) \tilde{\mathcal{J}}^*\left(-\frac{\tilde{\mathbf{x}}}{2}\right) \tilde{\mathcal{F}}\left(\frac{\tilde{\mathbf{x}}}{2}\right) \tilde{\mathcal{F}}^*\left(-\frac{\tilde{\mathbf{x}}}{2}\right) \right\rangle \quad (69)$$

where $\tilde{\zeta} = \mathbf{k}^- \cdot \tilde{\boldsymbol{\chi}}$. If we define a new function \tilde{f} by

$$\tilde{f}(\tilde{\mathbf{x}}) = \underbrace{\tilde{\mathcal{F}}^{(0)}}_{\tilde{f}^{(0)}} + \underbrace{(\tilde{\mathcal{F}}^{(0)} \tilde{\mathcal{J}}^{(1)}(\tilde{\mathbf{x}}) + \tilde{\mathcal{F}}^{(1)}(\tilde{\mathbf{x}}))}_{\tilde{f}^{(1)}(\tilde{\mathbf{x}})} \quad (70)$$

then σ^0 for a Lagrangian surface may be calculated by replacing $k_z^- \eta$ with $\tilde{\zeta}$ and \mathcal{F} with \tilde{f} in (51).

Note: in the calculations, the Lagrangian solution is replaced by an Eulerian solution for wavelengths shorter than 1.7 cm. This is done to avoid (unphysical) Stokes-like capillary waves.

REFERENCES

- [1] A. Komjathy, J. L. Garrison, and V. Zavorotny, ‘‘GPS: A new tool for ocean science,’’ *GPS World*, no. 4, pp. 50–56, Apr. 1999.
- [2] V. U. Zavorotny and A. G. Voronovich, ‘‘Scattering of GPS signals from the ocean with wind remote sensing application,’’ *IEEE Trans. Geosci. Remote Sensing*, vol. 38, pp. 951–964, 2000.
- [3] T. Elfouhaily, D. R. Thompson, and L. Linstrom, ‘‘Delay-doppler analysis of bistatically reflected signals from the ocean surface: Theory and application,’’ *IEEE Trans. Geosci. and Remote Sensing*, vol. 40, no. 3, pp. 560–573, 2002.
- [4] A. Thompson and C. H. Mathew, ‘‘PARIS mode in SAR mission,’’ presented at the *Proc. EUSAR2002*, Koln, Jun. 4–6, 2002.
- [5] H. Johnsen, G. Engen, and B. Chapron, ‘‘Validation of ASAR wave mode level2 product using WAM and buoy spectra,’’ presented at the *Proc. 2nd Workshop on Coastal and Marine Applications of SAR*, Longyearbyen, Sep. 8–12, 2003, Paper no. SP565.
- [6] P. W. Vachon and F. W. Dobson, ‘‘Wind retrieval from RADARSAT SAR images: selection of suitable C-band HH polarization wind retrieval model,’’ *Can. J. Remote Sensing*, vol. 26, no. 4, pp. 306–313, 2000.
- [7] B. Chapron, F. Collard, and V. Kerbaol, ‘‘Satellite synthetic aperture radar sea surface Doppler measurements,’’ presented at the *Proc. 2nd Workshop on Coastal and Marine Applications of SAR*, Longyearbyen, Sep. 8–12, 2003, SP565.
- [8] G. R. Valenzuela, ‘‘Theories for the interaction of electromagnetic and oceanic waves, a review,’’ *Bound.-Layer Meteorol.*, vol. 31, pp. 61–85, 1978.
- [9] —, ‘‘Depolarization of EM waves by slightly rough surfaces,’’ *IEEE Trans. Antennas Propag.*, vol. AP-15, no. 4, pp. 552–557, 1967.
- [10] A. Stogryn, ‘‘Electromagnetic scattering from rough finitely conducting surfaces,’’ *Radio Sci.*, vol. 2, no. 4, pp. 415–428, 1967.
- [11] P. J. Lynch, ‘‘Curvature corrections to rough surface scattering at high frequency,’’ *J. Acoust. Soc. America*, vol. 47, pp. 804–825, 1970.
- [12] E. Rodriguez, ‘‘Beyond the Kirchhoff approximation,’’ *Radio Sci.*, vol. 24, pp. 681–693, 1989.
- [13] —, ‘‘Beyond the Kirchhoff approximation II. Electromagnetic scattering,’’ *Radio Sci.*, vol. 26, pp. 121–132, 1991.
- [14] E. Rodriguez and Y. Kim, ‘‘A unified perturbation expansion for surface scattering,’’ *Radio Sci.*, vol. 27, no. 1, pp. 79–93, 1992.
- [15] M. I. Charnotskii and V. I. Tatarskii, ‘‘Tilt-invariant theory of rough-surface scattering. I,’’ *Waves in Random Media*, vol. 5, no. 4, pp. 361–380, 1995.

- [16] A. G. Voronovich, "Small-slope approximation in wave scattering from rough surfaces," *Sov. Phys. JETP*, vol. 62, no. 1, pp. 65–70, 1985.
- [17] —, *Wave Scattering From Rough Surfaces*, ser. Springer Series on Wave Phenomena. Berlin, Germany: Springer, 1994.
- [18] —, "Small-slope approximation for electromagnetic wave scattering at a rough interface of two dielectric half-spaces," *Waves in Random Media*, vol. 4, pp. 337–367, 1994.
- [19] T. Elfouhaily, M. Joelson, S. Guignard, and D. R. Thompson, "Analytical comparison between the surface current integral equation and the second-order small-slope approximation," *Waves in Random Media*, vol. 13, no. 3, pp. 165–176, 2003.
- [20] T. Elfouhaily, S. Guignard, and D. R. Thompson, "Formal tilt invariance of the local curvature approximation," *Waves in Random Media*, vol. 13, no. 4, p. L7, 2003.
- [21] T. Elfouhaily, S. Guignard, R. Awadallah, and D. R. Thompson, "Local and nonlocal curvature approximation: a new asymptotic theory for wave scattering," *Waves in Random Media*, vol. 13, no. 4, pp. 321–338, 2003.
- [22] J. A. Stratton, *Electromagnetic Theory*. New York: McGraw-Hill, 1941.
- [23] A. Ishimaru, *Electromagnetic Wave Propagation, Radiation, and Scattering*. New York: Prentice-Hall, 1991.
- [24] M. F. Chen and A. K. Fung, "A numerical study of the regions of validity of the Kirchoff and small perturbation rough surface models," *Radio Sci.*, vol. 23, no. 2, pp. 163–170, 1988.
- [25] J. R. Apel, "An improved model of the ocean surface wave vector spectrum and its effects on radar backscatter," *J. Geophys. Res.*, vol. 99, no. C8, pp. 16 269–16 291, 1994.
- [26] A. Bentamy, Y. Quilfen, P. Queffelec, and A. Cavanié, "Calibration and Validation of ERS-1 Scatterometer," *Inst. Fr. Rech. pour l'Exploit. de la Mer (IFREMER)*, Brest, France, 1994.
- [27] A. C. M. Stoffelen and D. L. T. Anderson, "Scatterometer data interpretation: Estimation and validation of the transfer function: Cmod4," *J. Geophys. Res.*, vol. 102, no. C3, pp. 5767–5780, 1997.
- [28] D. Thompson, T. Elfouhaily, and B. Chapron, "Polarization ratio for microwave backscattering from ocean surface at low to moderate incidence angles," presented at the *Proc. IGARSS'98*, Seattle, WA, Jul. 6–10, 1998.
- [29] T. M. Elfouhaily, "Modèle couple vent/vagues et son application à la télédétection par micro-onde de la surface de la mer," *University Paris 7*, Nov. 20, 1996.
- [30] I. S. Gradshteyn and I. M. Ryzhik, *Table of Integrals, Series and Products*, 6th ed. New York: Academic Press, 2000.
- [31] L. M. Brekhovskikh, *Waves in Layered Media*. New York: Academic Press, 1960.
- [32] C. T. Tai, *Dyadic Green's Functions in Electromagnetic Theory*. New York: Intext Educational Publishers, 1971.
- [33] T. Elfouhaily, B. Chapron, K. Katsaros, and D. Vandemark, "A unified directional spectrum for long and short wind-driven waves," *J. Geophys. Res.*, vol. 102, no. C7, pp. 15 781–15 796, 1997.
- [34] V. Kudryavtsev, D. Hauser, G. Gaudal, and B. Chapron, "A semiempirical model of normalized radar cross-section of the sea surface," *J. Geophys. Res.*, vol. 108, no. C3, p. 8054, 2003.
- [35] S. H. Gjøvsund, "A Lagrangian model for irregular waves and wave kinematics," *J. Offshore Mechanics Arctic Eng.*, vol. 125, pp. 94–100, 2003.

Geir Engen received the M.S. and Ph.D. degrees from the University of Tromsø, Tromsø, Norway, in 1991 and 1997, respectively.

In 1992, he visited IFREMER for two months and NASA Goddard Space Flight Center, Maryland, from October 1993 to September 1994. From 1997 to 1999, he worked as a Guest Scientist at the Norwegian Defence Research Establishment (FFI), and again in 2001 for six months as a Senior Research Scientist, before he joined Norut IT. His main interest at present is within EM scattering from ocean surfaces and SAR imaging of wind, waves and current.

Ida Friestad-Pedersen received the M.Sc. degree in mathematics from the University of Tromsø, Tromsø, Norway, in 2002.

In 2002, she joined Norut IT, Tromsø, as a Ph.D. student working within radar imaging of ocean surface phenomena.

Harald Johnsen received the M.Sc. degree in 1981 and the Ph.D. in 1984 from the University of Tromsø, Tromsø, Norway.

After graduating, he worked two years at the Auroral Observatory in Tromsø before joining Norut IT, Tromsø, in 1986 as a Research Scientist within the Earth Observation Group. From 1994 to 2002, he was the Research Manager at the same institution with responsibility for the remote sensing activities. His main research interest at present is within SAR ocean applications and SAR interferometry applications.

Tanos Elfouhaily is with the Division of Applied Marine Physics, University of Miami Rosenstiel School of Marine and Atmospheric Science, Miami, FL. His main research interests are remote sensing, surface waves, electromagnetic waves, and polarimetry.